Functional Genomics of the Rapidly Replicating Bacterium Vibrio Natriegens by CRISPRi

Supplementary Information for

Functional genomics of the rapidly replicating bacterium *Vibrio natriegens* by CRISPRi

Henry H. Lee[1], Nili Ostrov[1], Brandon G. Wong[2], Michaela A. Gold[3], Ahmad S. Khalil[2,4], George M. Church[1,4]

Supplementary materials provided in this document:

Supplementary Discussion

Plasmid stability and yield

Initial transformations with *E. coli* plasmids carrying constitutively-expressing GFP yielded variability in colony size and fluorescence, suggestive of plasmid instability [1]. Instead, we found that a plasmid based on the broad-host range RSF1010 origin [2] yielded transformants more consistent in morphology and fluorescence [2] (**Supplementary Figure 6)**. We developed a high efficiency method for introduction of recombinant DNA into *V. natriegens*. This protocol can generate electrocompetent cells in 2 hours which are also suitable for direct long-term storage at -80°C. Transformation efficiencies up to to $2x10^5$ CFU/μg can be achieved and transformants can be obtained with as little as 10ng plasmid DNA. Transformants can be visualized and picked after 5 hours of plating. Furthermore, 2μg of plasmid DNA can be isolated within 5 hours of growth, ~2.5x more than equivalent *E. coli* culture (**Supplementary Figure 7**).

Harnessing the CTX replicon as a new *V. natriegens* plasmid

In search of additional stable replicons, we turned to bacteriophages. Like the coliphage M13, whose replicative form (RF) served as a basis for early *E. coli* plasmids, we used the CTX vibriophage [3]. Transformation of CTX RF in *V. natriegens* yielded robust transformants. We thus constructed a new shuttle plasmid., pCTX-R6K, by fusing CTX replication genes with the conditionally replicating R6K origin for cloning in *E. coli*.

We further tested the infectivity of CTX on *V.* natriegens. Importantly, we found that the CTX bacteriophage was >100-fold less infective of *V. natriegens* compared to *V. cholerae* O395. Furthermore, we could not detect production of infective viral CTX particles in the supernatant of *V. natriegens* transformants which had undergone direct electroporation of CTX replicative form (**Supplementary Figure 8**), showing that CTX viral particles are either not produced or not functionally assembled in *V. natriegens*. Given the low rates of infectivity and the fact that CTX virions are not found in high-titers in the environment, we conclude *V. natriegens* is an unlikely host for the propagation of CTX phage [4]. These tests further support the Biosafety Level 1 (BSL-1) designation for *V. natriegens* as generally safe biological agent.

Transposon mutagenesis saturation and characterization

We observed low saturation of transposon mutagenesis in *V. natriegens*, with only 47.7% of genes containing one insertion and 23.4% containing ≥2 insertions (**Supplementary Table 8**). Further analysis revealed that a large percentage of the transposon library sequencing reads mapped to the transposon backbone. This is indicative of genomic integration of the suicide transposon vector since no plasmids could be extracted from *V. natriegens* transconjugants, and direct electroporation of the transposon plasmid alone into *V. natriegens* did not produce any detectable transformants. Interestingly, genomic integration of a suicide transposon vector

following conjugation in *V. cholerae* strains has been observed, and the underlying mechanisms of this activity is not well understood. Deeper investigation into these integration events may improve the fidelity of transposon mutagenesis in *V. natriegens*.

We also analyzed transposon mutant colonies in greater detail by whole genome sequencing. When grown without antibiotic selection for the transposon, we were unable to find sequencing reads that mapped to the transposon, indicating instability and excision of this genomic element. Additionally, we found that some mutants carried genomic sequences which mapped to portions or all of the transposon suicide vector, including the Himar1 transposase, the ampicillin marker, and the oriT and R6K origin. These excisions and integrations greatly impede high-throughput identification of insertion locations since no common sequence can be used to determine the junction between integrated DNA and genomic DNA. Deep sequencing of specific mutants can, however, enable identification of the genetic perturbation underlying a specific phenotype.

CRISPRi of *recQ* helicase

We note that *recQ* helicase (PEG.2665), a highly conserved protein involved in genome maintenance including replication, repair and transcription [5], showed the highest positive beta score across all tested conditions (**Supplementary Table 5**), suggesting its inhibition enables a competitive advantage under the screening conditions. When comparing the growth rate of single-gRNA inhibition of *recQ* to that of *flgC* (neutral gene) or GFP under non competitive conditions, we found that while all strains displayed similar growth rates and morphologies, *recQ* inhibition resulted in significantly shorter lag phase (**Supplementary Figure 17**). This result, which corroborates the pooled experiment data, is also in line with previous observations that dCas9 inhibition manifests as differences in lag phase, rather than growth rates [6]. Interestingly, we observed no change in lag phase in strains where recQ was completely deleted (**Supplementary Figure 17d**). We thus conclude that *recQ* inhibition relieves growth impairment caused by dCas9. Further work is required to elucidate the effect of positive-scoring genes in this system.

Supplementary Figures

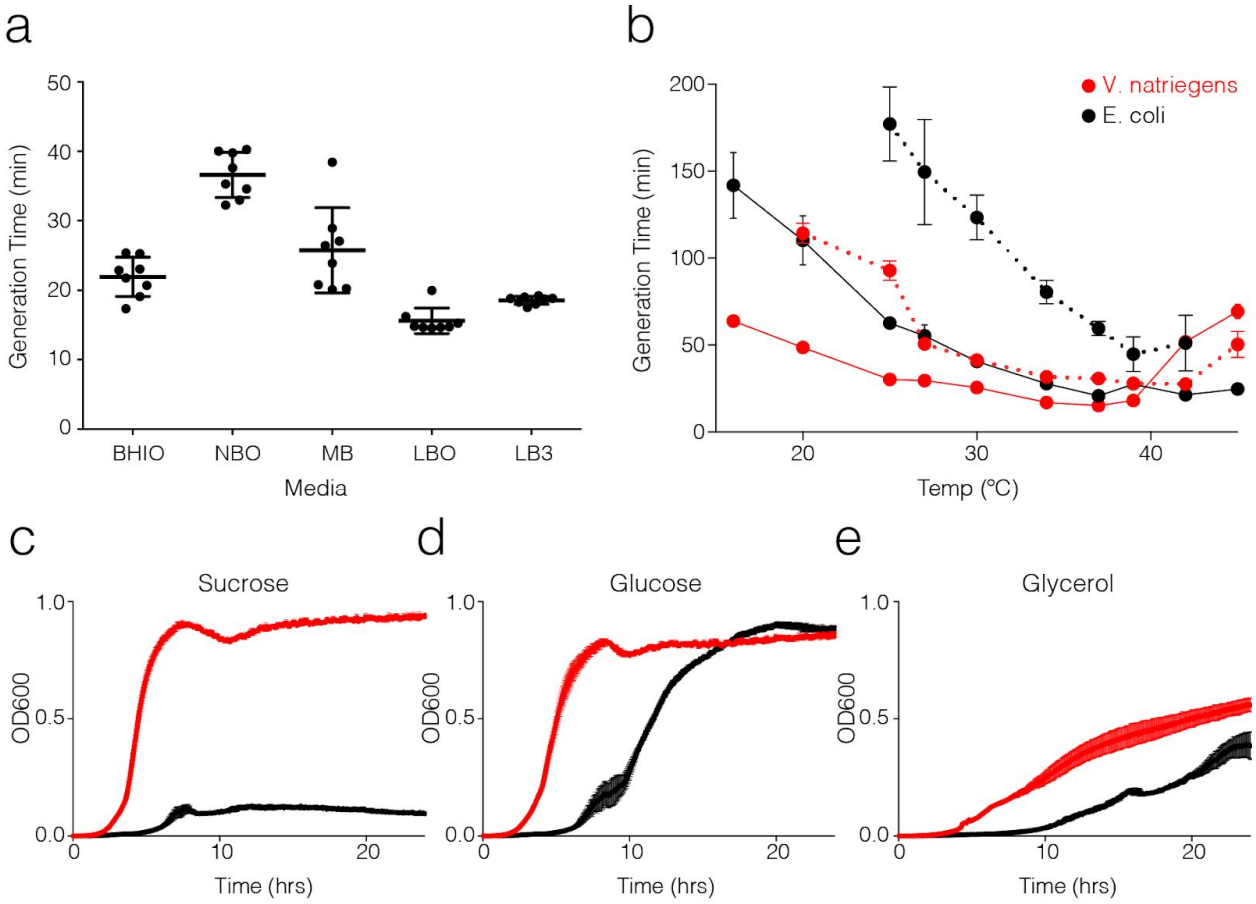

Supplementary Figure 1. Media and growth measurements. (a) Bulk growth measurements of *V. natriegens* at 37°C in rich media. Brain Heart Infusion (BHIO), Nutrient Broth (NBO), and Lysogeny Broth (LBO) were supplemented with 1.5% (w/v) final Ocean Salts. No additional salts were added to Marine Broth (MB). LB3 is Lysogeny Broth with 3% (w/v) NaCl. Data shown are mean±SD (N=8 technical replicates). (b) Growth measurements of *V. natriegens* (red) and *E. coli* (black) at the indicated temperature. Generation time was measured in bulk using rich media (solid line, LB3 and LB, respectively) or minimal media (dotted line, M9-glucose with or without 2% (w/v) NaCl, respectively). Data shown are mean±SD (N=24 technical replicates). Generation time data also provided in **Supplementary Table 1**. (c-e) Bulk growth measurement of *V.natriegens* (red) and *E.coli* (black) in minimal media (M9 salts) with the indicated carbon sources at 0.4% (w/v) final concentration. For *V.natriegens*, 2% (w/v) NaCl was added. Data shown are mean±SD (N=12 technical replicates). Experiments were repeated twice independently with similar results.

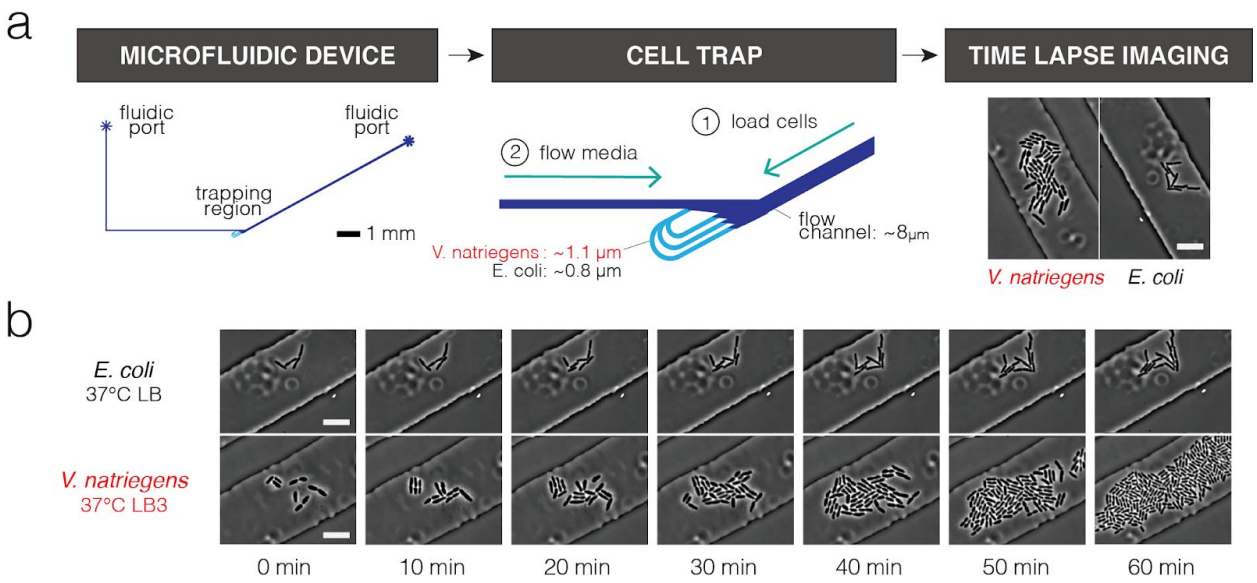

Supplementary Figure 2. Microfluidic single-cell growth rate measurements. (a) Microfluidic chemostat devices were designed to keep cells growing in a monolayer. Two different devices with altered cell trapping heights were used to image *V. natriegens* and *E. coli*. (b) Side-by-side comparison of optimal growth conditions of each cell type (N=3 independent experiments). Images acquired at 100x magnification, scale bar 10 μm.

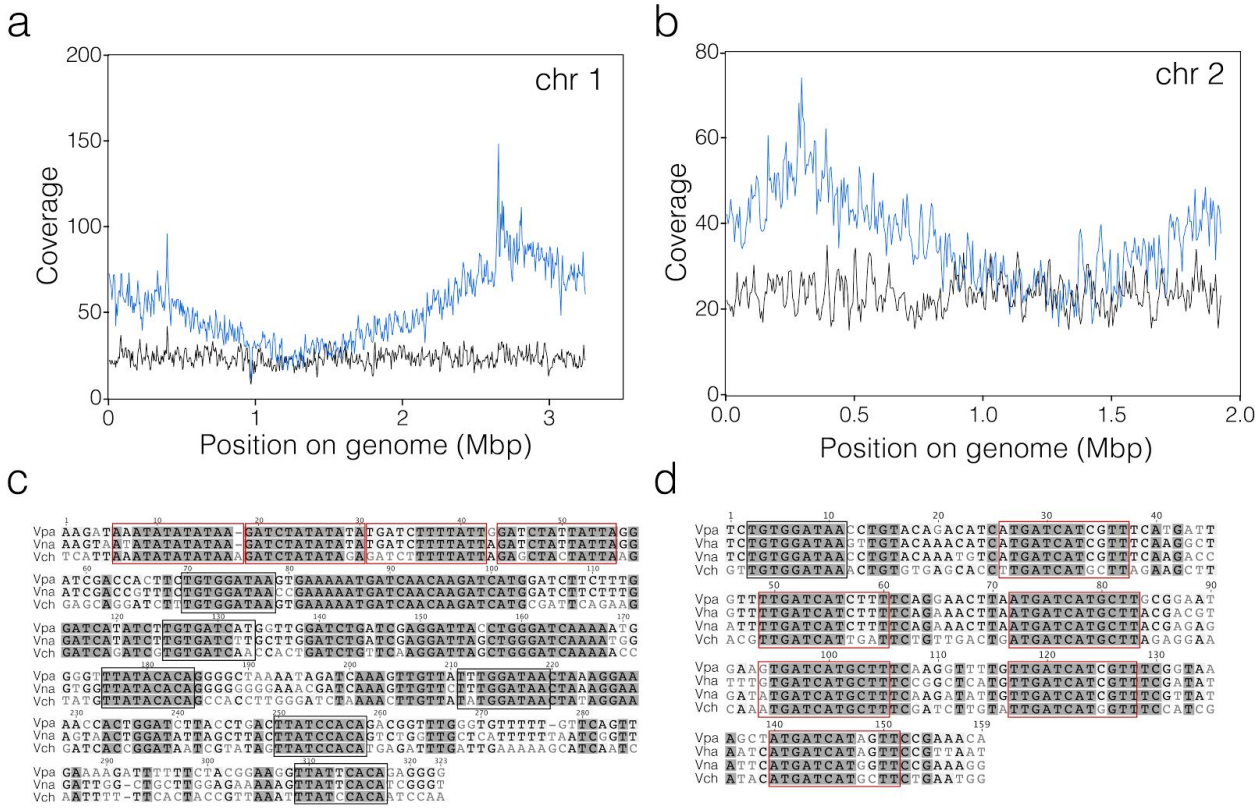

Supplementary Figure 3. Determination of replication origin and terminus. (a, b) *V. natriegens* chromosome sequencing coverage at exponential (blue) and stationary phase (black). Unfiltered raw reads are shown which map to the genome. (c) Alignment of Origin of replication sequence for chromosome 1. The putative origin of replication for chromosome 1 ($OriCI_{Vn}$) contains homologous sequences to experimentally determined OriCI of related *Vibrio* species [7,8]. The following motifs are labeled: AT cluster and AT-rich 13-mer repeats (red), DnaA boxes (black). Vna - *V. natriegens* ATCC 14048 (SAMN03178087), Vpa - *V. parahaemolyticus* O1:K33 (CP006008.1), Vch - *V. cholerae* O395 (AY034431.1). (d) Alignment of Origin of replication sequence for chromosome 2. The predicted origin of replication for chr2 ($OriCII_{Vn}$), which closely correlated with GC-skew prediction, did not share sequence similarity with other experimentally determined OriCII. However, as shown here, we identified consensus OriCII sequences ~20 kb downstream of the locus predicted by GC-skew, as previously shown for *V. cholerae* [9]. DnaA box (black) and repeats (red) are shown. Vpa - *V. parahaemolyticus* RIMD 2210633 (Accession: NC_004605.1), Vch -*V. cholerae* O1 biovar El Tor str. N16961 (NC_002506.1), Vha - *V. harveyi* ATCC 33843 (NZ_CP009468.1).

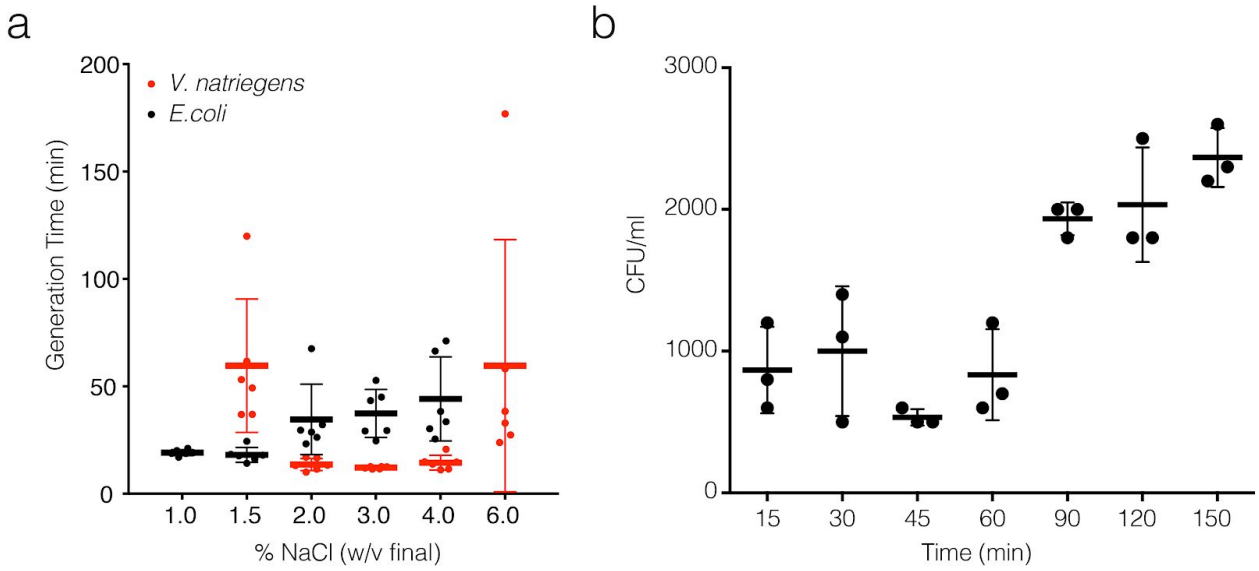

Supplementary Figure 4. Optimization of conjugation conditions between *E. coli* and *V. natriegens* for transposon mutagenesis experiments. (a) Cell viability for both organisms was determined with increasing amount of salt in growth media. *V. natriegens* did not grow in LB - 1% (w/v) final NaCl. Data are shown as mean±SD (N=6 technical replicates). (b) Number of transconjugants resulting from suicide transposon vector as a function of conjugation time. Data are shown as mean±SD (N=3 technical replicates). Experiments were repeated twice independently with similar results.

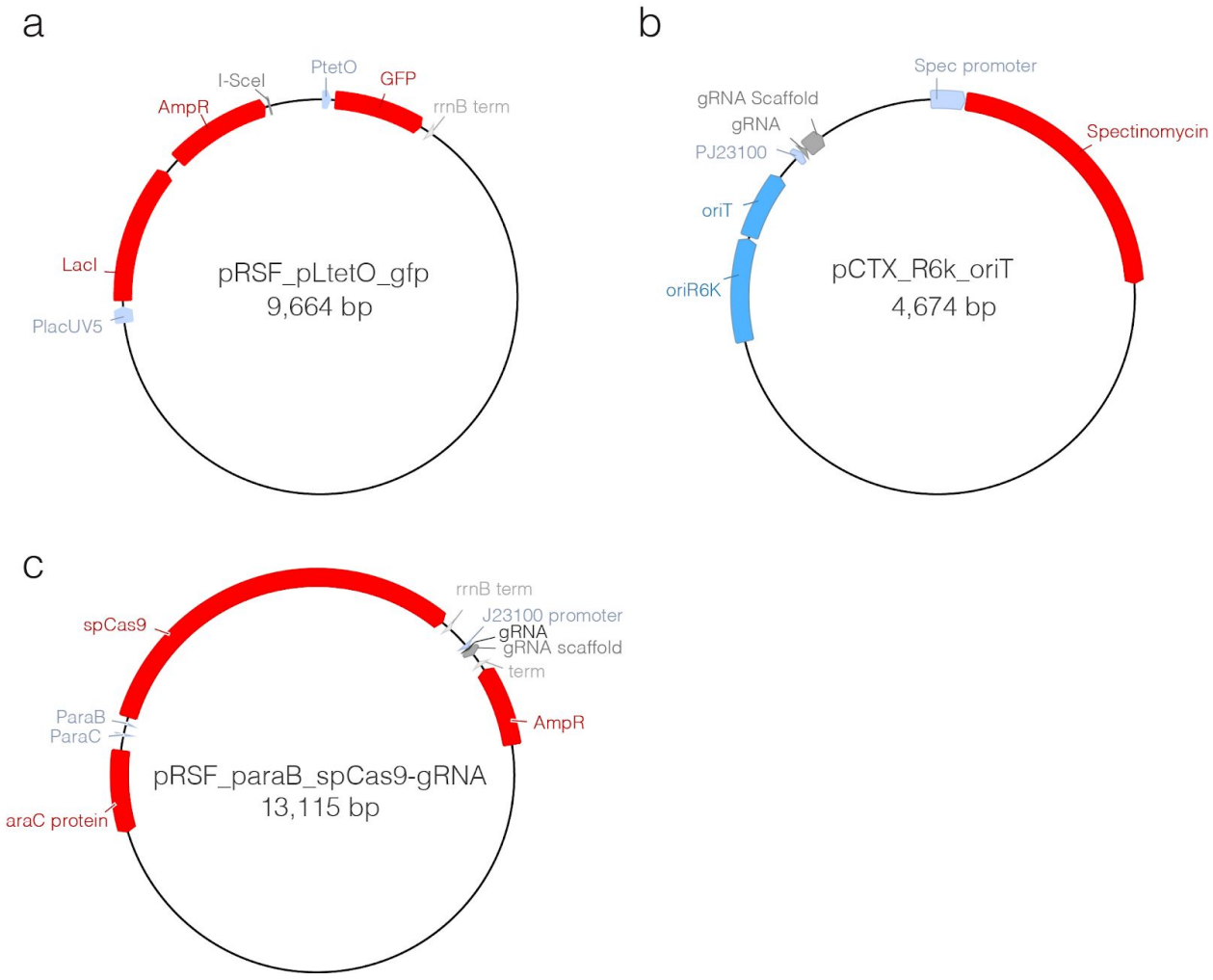

Supplementary Figure 5. Plasmid maps. (a) pRSF-pLtetO-GFP (b) pCTX-R6K-gRNA. (c) pRSF-paraB-spCas9-gRNA. (See also **Supplementary Table 4**).

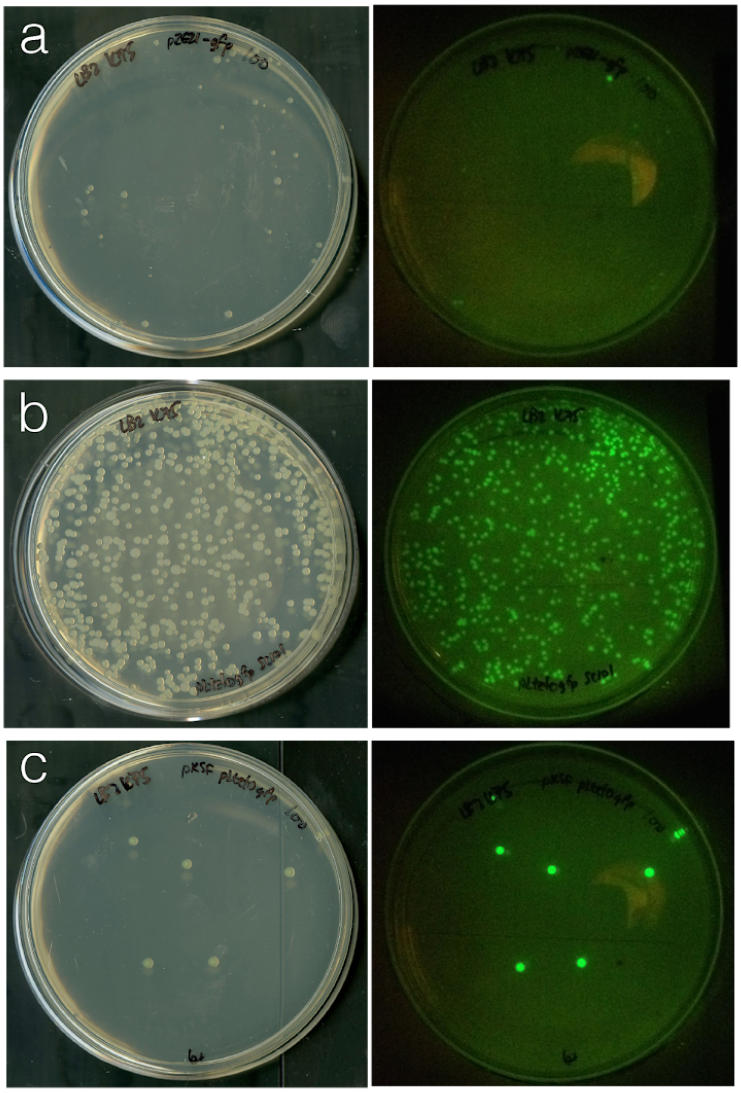

Supplementary Figure 6. Testing plasmid transformation. Bright field (left) and fluorescence images (right) of *V. natriegens* colonies transformed with plasmids carrying constitutive GFP expression cassette pLtetO-GFP, using the following replicons (a) colE1 (b) SC101 (c) RSF1010. Representative images are shown. Experiments were repeated twice independently with similar results.

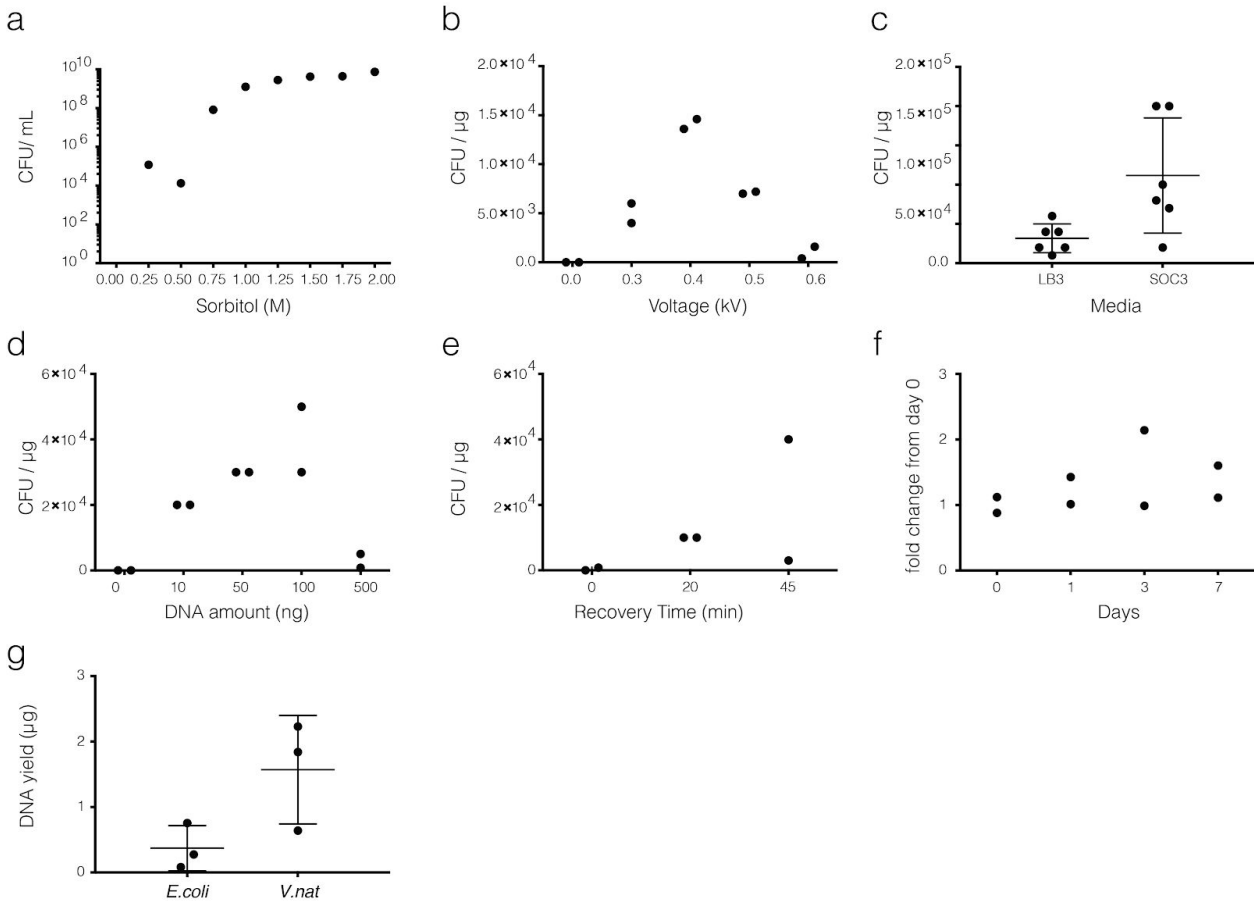

Supplementary Figure 7. Optimization of electroporation conditions. (a) Cell viability in sorbitol, which was used as an osmoprotectant (representative data, N=1). Transformation efficiencies were optimized for the following criteria: (b) Voltage. (c) Recovery media. (d) Amount of input plasmid DNA. (e) Recovery time. (f) competent cell storage: transformation efficiencies of electrocompetent cells stored at -80°C over time. (day 0: freshly prepared electrocompetent cells). Unless otherwise indicated, experiments for panels b-f were performed using 50ng of plasmid pRSF-pLtetO-gfp with recovery time of 45min at 37°C in SOC3 media (N=2 technical replicates). (g) Plasmid yield in *V. natriegens*. Single colonies of *V. natriegens* or *E. coli* were used to inoculate 3mL liquid LB3 or LB, respectively. Cultures were grown for 5 hours at 37°C and plasmid DNA was extracted and quantified. Data are shown as mean±SD (N=3 biological replicates). Experiments were repeated twice independently with similar results.

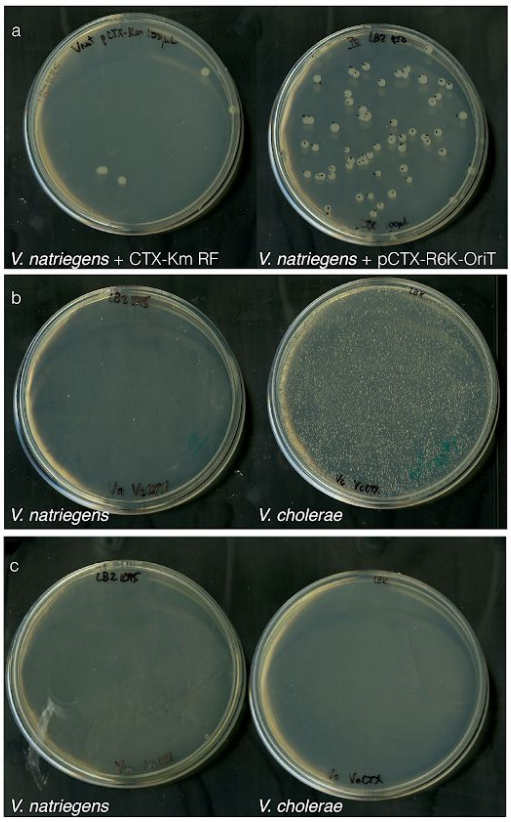

Supplementary Figure 8. CTX bacteriophage replication and infectivity. The CTX origin of replication was used to construct plasmid pCTX-R6K-OriT. (a) Transformation of *V. natriegens* cells using replicative form of CTX, pCTX-Km (left) or plasmid pCTX-R6K-OriT (right). (b) Transduction of *V. natriegens* (left) or *V. cholerae* O395 (right) by bacteriophage CTX-Km$^{Vc}\Phi$ produced by *V. cholerae* O395. (c) Transduction of *V. natriegens* (left) and *V. cholerae* O395 (right) by bacteriophage CTX-Km$^{Vn}\Phi$ produced by *V. natriegens*. Representative images are shown. Experiments were repeated twice independently with similar results.

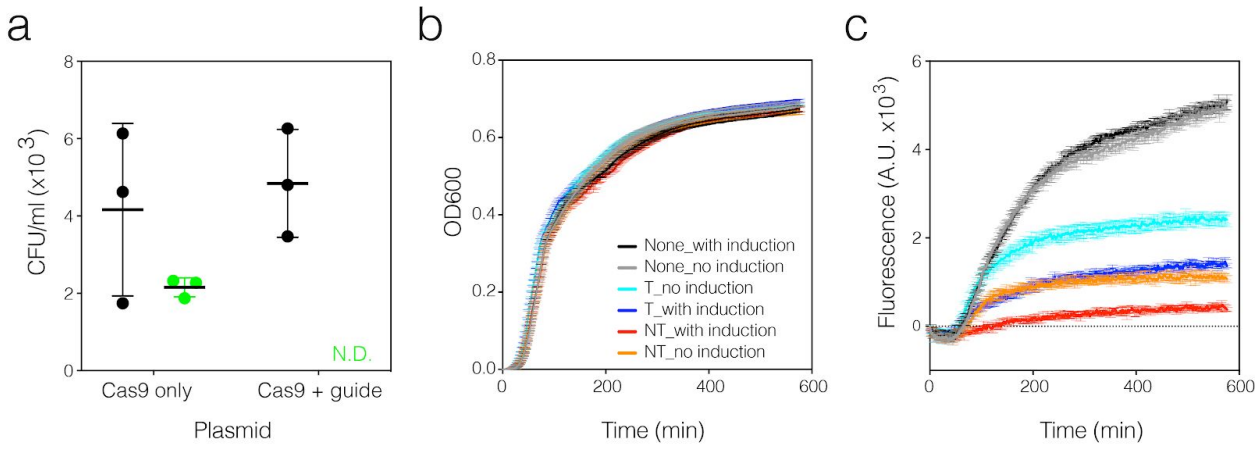

Supplementary Figure 9. CRISPR/Cas9 and dCas9 functionality. (a) Cas9 nuclease activity. Plasmid pRSF-pAra-Cas9-gRNA expressing both Cas9 nuclease and a GFP-targeting guide was electroporated into wild type (black) or reporter strain with genomically integrated GFP (green). In the presence of both nucelease and gRNA, reporter strain colonies were not detected (N.D.). No arabinose was added for induction of Cas9. Data are shown as mean±SD (N=3 technical replicates). (b-c) Nuclease-deficient dCas9 activity. Reporter strain carrying genomically integrated pLtetO-GFP cassette was transformed with plasmid pRSF-pAra-dCas9-gRNA expressing arabinose-induced dCas9 and gRNA. Optical density (b) and GFP fluorescence (c) are shown for plasmid lacking any gRNA ('None'), guide targeting GFP template strand ('T'), and guide targeting GFP non-template strand ('NT') strand. dCas9 induction was performed using 1mM arabinose. Data are shown as mean±SD (N=4 technical replicates). Experiments were repeated twice independently with similar results.

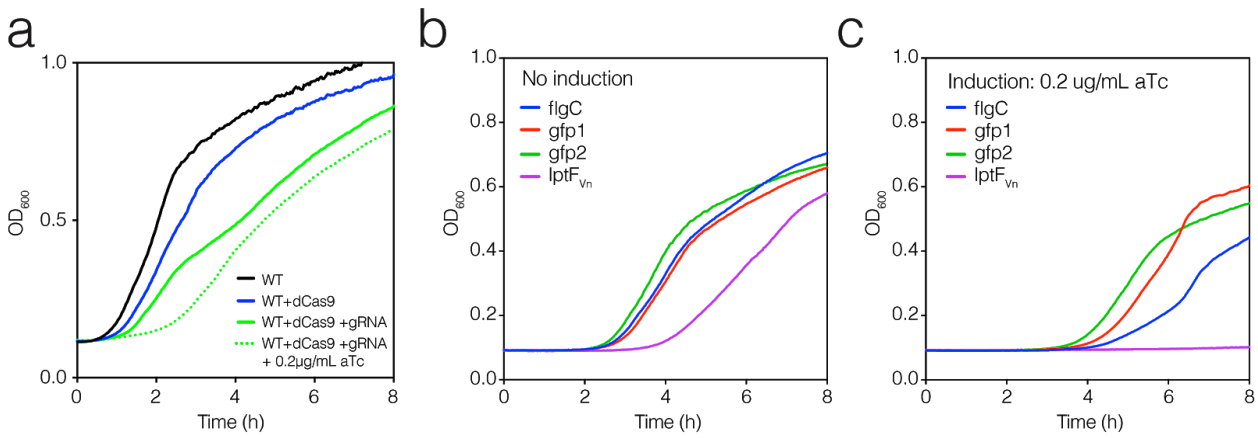

Supplementary Figure 10. Toxicity of dCas9 under aTc inducible promoter. (a) Growth curves for wild type *V. natriegens*, wild type strain carrying only dCas9 plasmid (pdCas9-bacteria[10]), or wild type strain carrying both dCas9 (pdCas9-bacteria) and gRNA targeting GFP with or without induction of dCas9 (pCTX-R6K-gRNA). Data are shown as mean (N=4 technical replicates). (b-c) Growth curves for strains carrying both dCas9 (pdCas9-bacteria) and gRNA (pCTX-R6K-gRNA) targeting inhibition of the indicated genes, without induction of dCas9 (b) or with 0.2 µg/mL of aTc for induced expression of dCas9 (c). All strains grown in LB3 at 37°C. Data are shown as mean (N=2 technical replicates). Experiments were repeated twice independently with similar results.

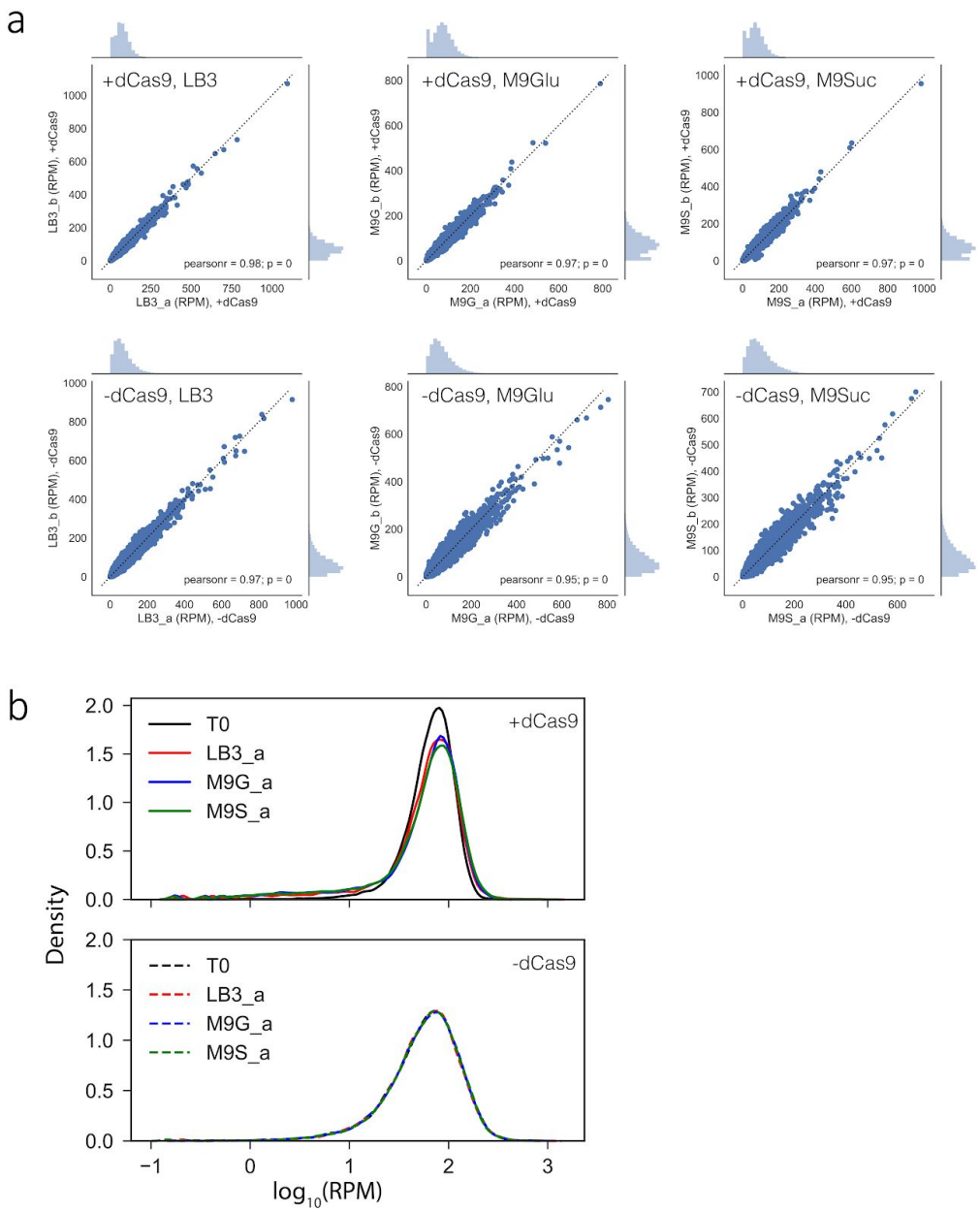

Supplementary Figure 11. Pooled genome-wide CRISPRi screen in minimal and rich media. Library was grown in LB3, M9+0.4% glucose (M9G), or M9+0.4% sucrose (M9S). (a) Correlation of gRNA counts, expressed as reads per million (RPM), between biological replicates from each media condition with (top) or without dCas9 (bottom). Dotted line is x=y. The p-value for the Pearson's correlation is computed with a two-tailed Student's t-test with degrees of freedom n-2 where n = 13587. (b) Distribution of log10-transformed gRNA abundance for the initial library (black), after competitive growth in LB3 (red), M9-Glucose (blue) or M9-Sucrose (green). Top: gRNA abundance in the presence of dCas9. Bottom: gRNA abundance in the absence of dCas9. Representative distribution is shown from one of two replicates.

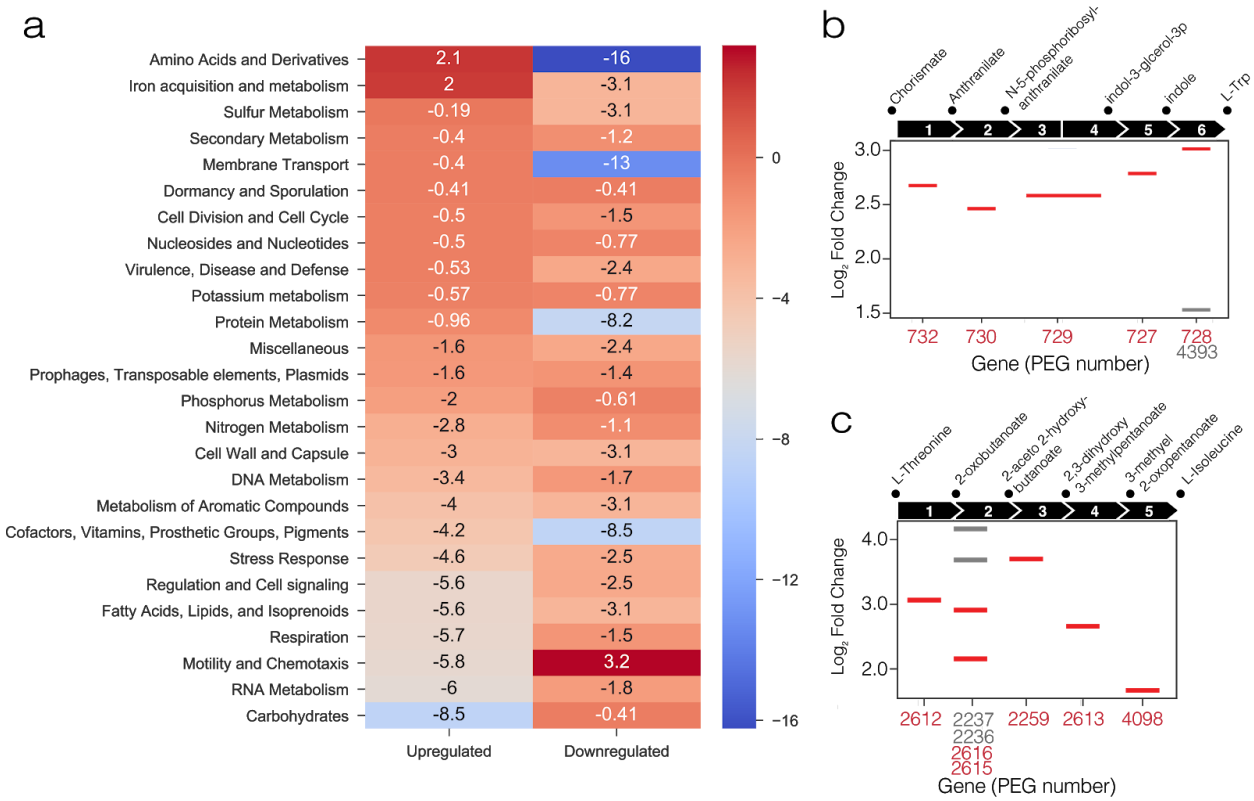

Supplementary Figure 12. Functional genes identified by genome-wide CRISPRi screen in minimal media. (a) Heatmap showing enrichment (red) or depletion (blue) of each RAST category for significantly differentially expressed genes in minimal media (M9) vs. rich media (LB3). Statistics are derived from one-tailed hypergeometric test assuming independence between categories for enrichment and depletion for differentially upregulated (N=756 genes) and downregulated (N=661 genes) in minimal media vs. rich media. False discovery rate (FDR) controlled with Benjamini-Hochberg. Values shown are obtained by summing the $\log_{10}$(FDR) from both enrichment and depletion. (b-c) Functional genes identified in CRISPRi screen were assigned to tryptophan and Isoleucine biosynthetic pathways. Fold change in expression between LB3 and M9 media is shown for each gene. For each pathway step, all computationally assigned protein encoding genes (PEG) are listed. Functional genes identified by CRISPRi are shown in red. (b) Tryptophan (L-Trp) biosynthetic pathway, starting from Chorismate. (c) Isoleucine biosynthetic pathway, starting from L-threonine.

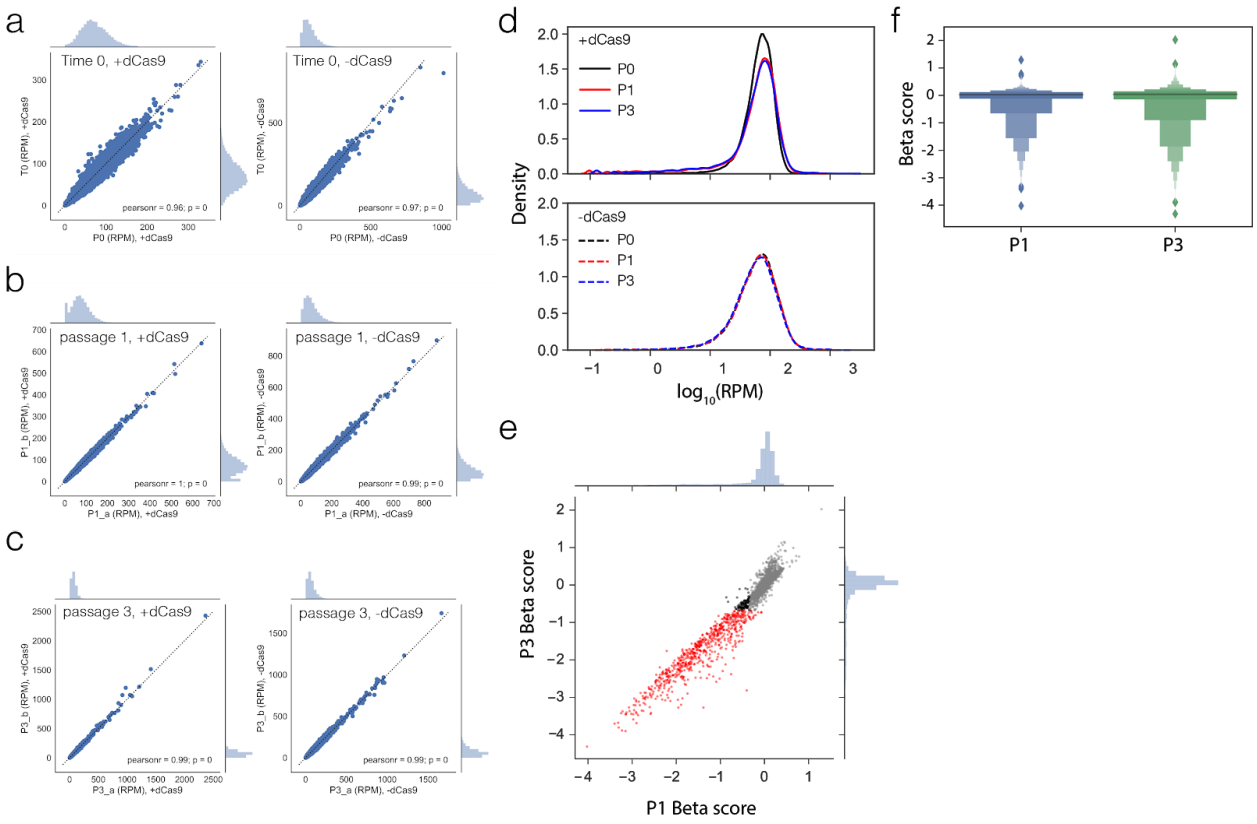

Supplementary Figure 13. Pooled genome-wide CRISPRi screen with serial passaging in rich media. (a) Correlation of gRNA counts, expressed as reads per million (RPM), between the initial pool of two rich media experiments in the presence (left) and absence of dCas9 (right). (b) Correlation of gRNA counts between biological replicates for the first passage in rich media. (c) Correlation of gRNA counts between biological replicates for the third passage in rich media. For (a-c): the p-value for the Pearson's correlation is computed with a two-tailed Student's t-test with degrees of freedom n-2 where n = 13587. Dotted line indicates x=y. (d) Distribution of log10-transformed gRNA abundance at different media passages. Initial library (black), first passage (red, P1), and third passage (blue, P3). Representative distribution is shown from one of two replicates. (e) Beta scores for all genes in P1 and P3. The set of 587 core genes shown in red have significant beta scores in both passages. 100 genes shown in black were significant in P1 but not in P3. all other genes shown in grey. Histograms show distribution of all genes. (f) Median and distribution of beta scores for passage 1 (P1, blue) and passage 3 (P3, green). All genes (N=4565) are included.

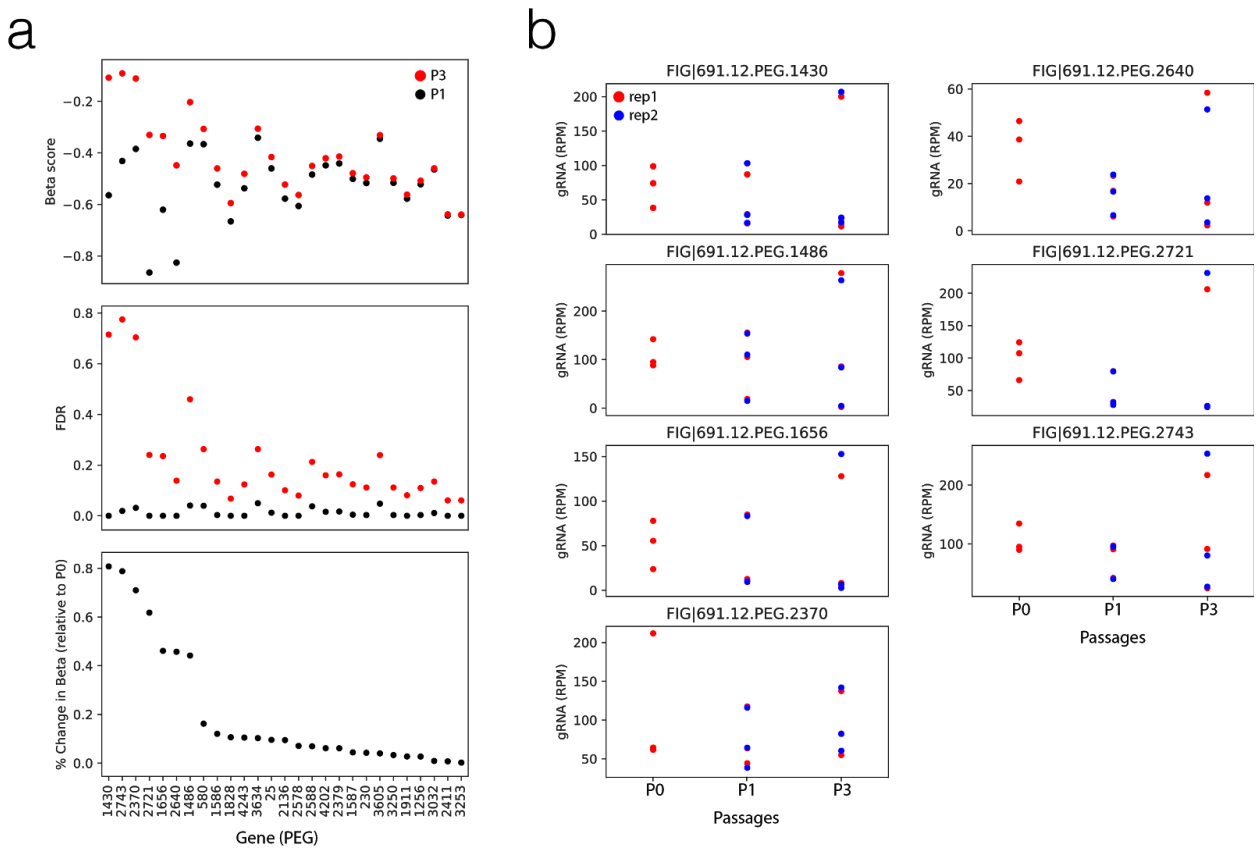

Supplementary Figure 14. Analysis of potential CRISPRi escapees by serial passaging in rich media. Cells were grown for 8 hours in LB3 at 37°C, then passaged twice by dilution in fresh media. The 27 genes which increase in beta score between the first and last passage are shown. (a) Beta score (top) and FDR (middle) for each gene in passage 1 (black) and passage 3 (red). Genes are listed as PEG number (see **Supplementary Table 5**). Bottom: percent change of beta score in passage 3 relative to passage 1. (b) single gRNA counts, normalized to reads per million (RPM), for 7 genes whose beta scores increase by more than 20% between passages (gene indicated as PEG number). Data shown for both experimental replicates (replicate 1 red; replicate 2 blue) in cell carrying gRNA and dCas9. P0 - prior to growth, P1 - first passage, P3 - third passage.

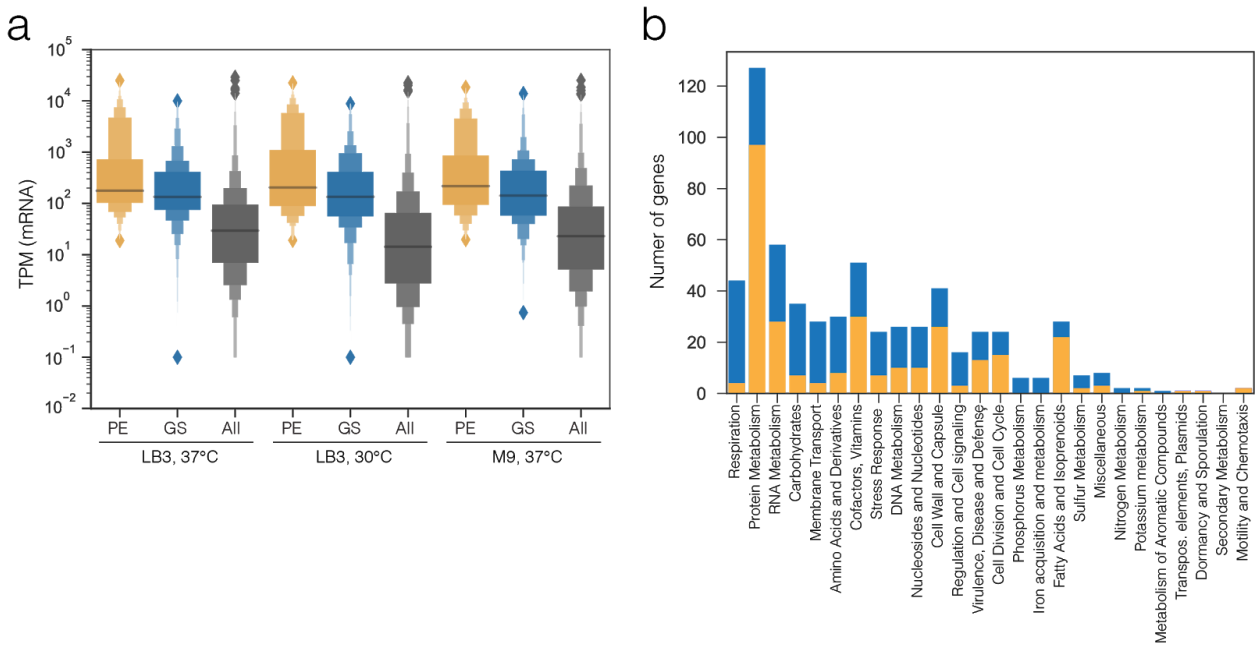

Supplementary Figure 15. Characterization of core genes. (a) Transcription levels of putative essential core genes (yellow, N=278), growth-supporting core genes (blue, N=309) and all library genes (gray, N=4578), as measured by RNA-seq under the indicated growth conditions as letter-value plots with median (b) Number of core genes in each RAST category, shown for putative essentials (yellow) and growth-supporting core genes (blue). We note 17% of core genes (89 of 523 genes) had no RAST category.

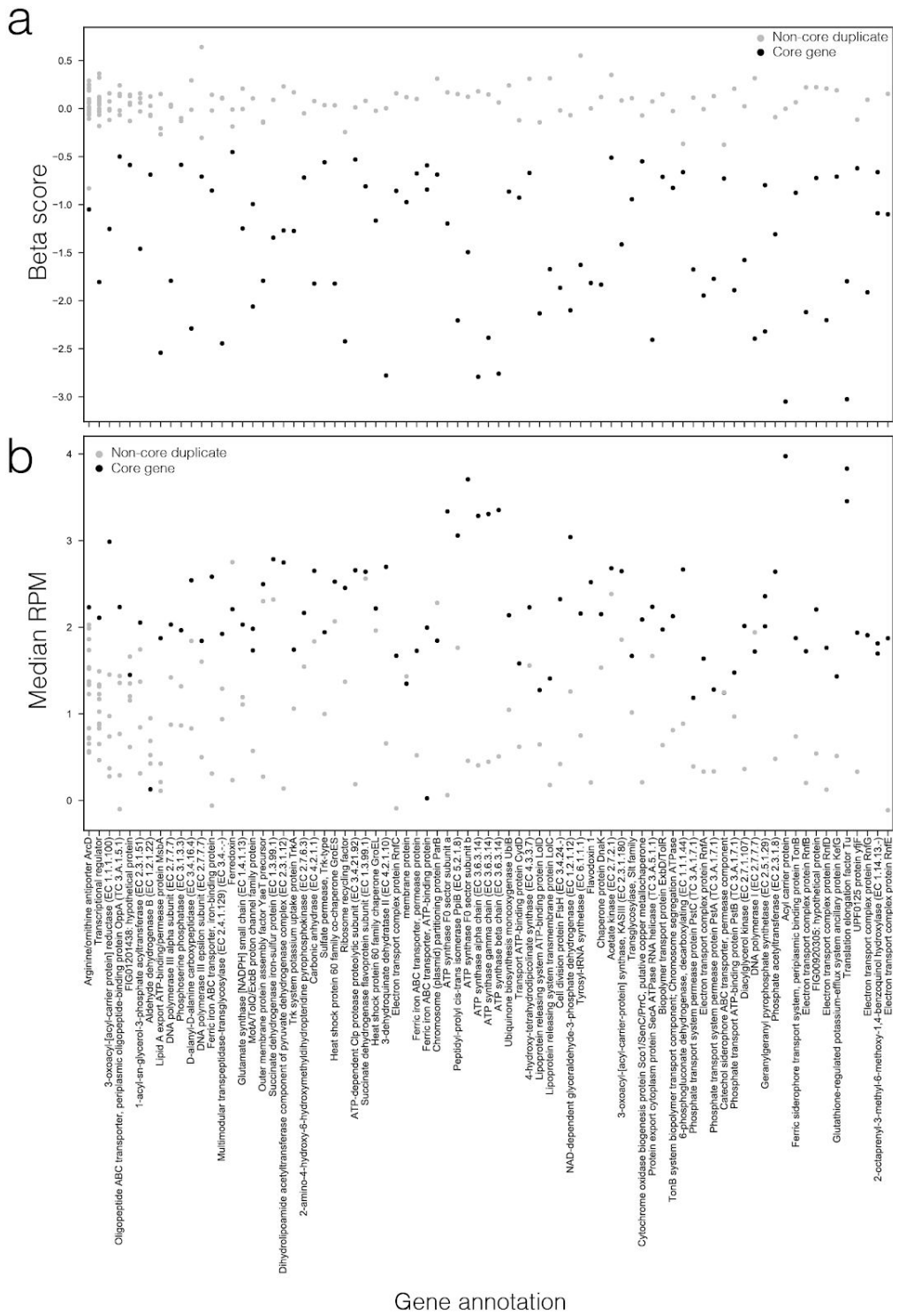

Supplementary Figure 16. Characterization of core gene duplications. (a) Beta score and (b) mRNA expression (expressed as median reads per million) are shown for all core genes for which one or more gene with identical annotation exists ('duplicates'). Core genes are shown in black. Non-core duplicates are shown in gray.

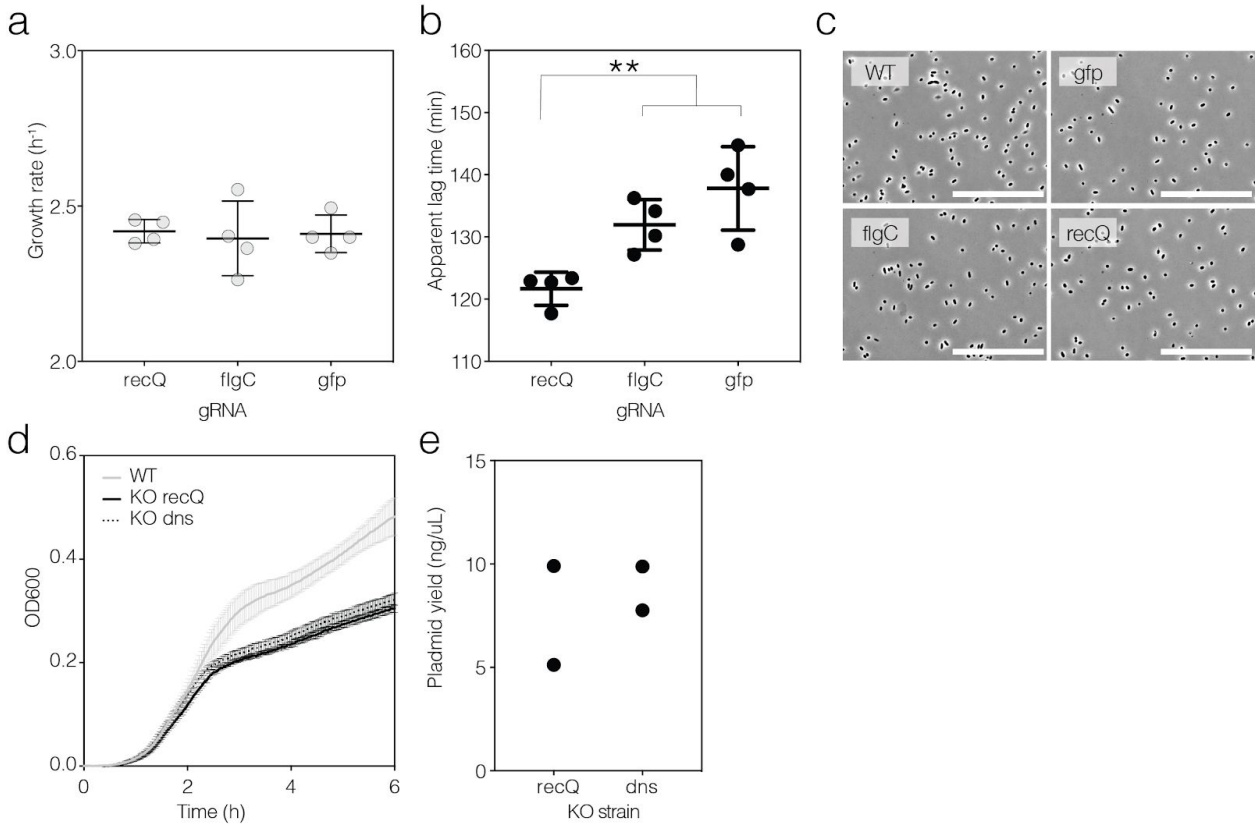

Supplementary Figure 17. Analysis of recQ helicase inhibition under non-competitive conditions. (a-c) analysis of cells carrying dCas9 (plasmid pRSF-ParaB-dCas9-gRNA) and single guides (plasmid pCTX-R6K-gRNA) for inhibition of recQ (PEG. 2665), flgC (PEG.1866), or gfp. Cells were grown individually in LB3 media at 37°C: (a) Growth rate. Data are shown as mean±SD (N=4 technical replicates). (b) Apparent lag time. Data are shown as mean±SD (N=4 technical replicates). Statistical significance is computed as an unpaired two-tailed t-test. ** denotes p<0.01: *recQ* vs. *gfp* (p = 0.0042), *recQ* and *flgC* (p=0.0055), *flgC* and *gfp* (p=0.1861). (c) Microscopy. A representative image of one biological replicate is shown for each condition. Scale bar = 200 μm (N=3 fields of view from the same biological sample). (d) Growth curves for wild type and single gene deletion for recQ or dns. Data are shown as mean±SD (N=4 technical replicates). (e) Plasmid yield from 1mL of overnight cultures of each knockout strain carrying the same pRSF vector (N=2 biological replicates).

	E. coli				*V. natriegens*			
	LB		**M9 Glucose**		**LB3**		**M9 Glucose +2% NaCl**	
Temp (°C)	**Generation time (mins)**	**Stdev**	**Generation time (mins)**	**Stdev**	**Generation time (mins)**	**Stdev**	**Generation time (mins)**	**Stdev**
16	141.8	19.0			63.8	2.6		
20	110.2	14.1			48.5	2.6	114.3	5.8
25	62.6	3.7	177.1	21.3	30.2	1.3	92.8	5.6
27	55.3	6.2	149.5	30.3	29.6	2.0	50.6	2.6
30	40.6	2.6	123.3	12.9	25.5	2.4	41.3	1.4
34	27.8	1.2	80.4	6.8	16.9	0.3	31.7	0.8
37	20.8	1.3	59.5	4.0	15.2	0.7	30.8	0.9
39	27.3	2.6	44.7	10.1	18.0	1.2	28.0	0.8
42	21.3	0.7	51.1	16.1	51.9	2.6	27.6	1.3
45	24.7	1.2			69.3	4.1	50.3	7.4

Supplementary Table 1. Generation time measurements for *V. natriegens* and *E.coli* (data plotted in supplementary Figure 1b). Generation time was measured in bulk using rich media (LB3 and LB, respectively) or minimal media (dotted line, M9 glucose. *V. natriegens* media supplemented with 2% (w/v) NaCl) (N=24 technical replicates).

Features of the *V. natriegens genome*	**chr1**	**chr2**
Size (bp)	3,248,023	1,927,130
G+C percentage	45.30%	44.70%
Total number of ORFs	2884	1694
Average ORF size (bp)	960	968
Number of rRNA operons (16S-23S-5S)	10	1
Number of tRNA	116	13
Genes with annotated function*	1607 (55.7%)	743 (43.8%)
Genes with unknown function**	1277 (44.3%)	951 (56.2%)

Supplementary Table 2. Major features of *V. natriegens* genome. RAST annotated *V. natriegens* strain ATCC 14048; RefSeq NZ_CP009977-8. *Genes annotated with a RAST category. ** Genes with no RAST category annotation

Codon	AA	Fraction	Frequency	Number	Codon	AA	Fraction	Frequency	Number
GCA	A	0.297	25.499	37529	CCA	P	0.394	15.616	22983
GCC	A	0.16	13.753	20241	CCC	P	0.072	2.874	4230
GCG	A	0.279	23.949	35248	CCG	P	0.222	8.823	12985
GCU	A	0.264	22.657	33346	CCU	P	0.311	12.355	18184
UGC	C	0.336	3.508	5163	CAA	Q	0.59	25.924	38155
UGU	C	0.664	6.917	10181	CAG	Q	0.41	18.009	26506
GAC	D	0.395	21.56	31732	AGA	R	0.098	4.332	6376
GAU	D	0.605	33.05	48643	AGG	R	0.03	1.313	1933
GAA	E	0.651	42.243	62172	CGA	R	0.146	6.458	9505
GAG	E	0.349	22.632	33310	CGC	R	0.266	11.729	17262
UUC	F	0.408	16.819	24754	CGG	R	0.033	1.467	2159
UUU	F	0.592	24.364	35858	CGU	R	0.427	18.836	27723
GGA	G	0.122	8.499	12508	AGC	S	0.192	12.683	18666
GGC	G	0.324	22.604	33268	AGU	S	0.181	11.938	17570
GGG	G	0.098	6.814	10029	UCA	S	0.191	12.587	18526
GGU	G	0.457	31.901	46952	UCC	S	0.078	5.125	7543
CAC	H	0.498	11.015	16212	UCG	S	0.123	8.12	11951
CAU	H	0.502	11.121	16367	UCU	S	0.235	15.539	22870
AUA	I	0.102	6.423	9454	ACA	T	0.226	12.092	17797
AUC	I	0.415	25.998	38263	ACC	T	0.277	14.826	21820
AUU	I	0.483	30.288	44578	ACG	T	0.233	12.489	18381
AAA	K	0.685	35.536	52302	ACU	T	0.265	14.195	20892
AAG	K	0.315	16.332	24037	GUA	V	0.22	15.973	23509
CUA	L	0.13	13.323	19608	GUC	V	0.187	13.608	20028
CUC	L	0.089	9.132	13440	GUG	V	0.256	18.586	27354
CUG	L	0.223	22.871	33661	GUU	V	0.336	24.427	35952
CUU	L	0.181	18.499	27227	UGG	W	1	12.647	18614
UUA	L	0.195	19.94	29348	UAC	Y	0.561	16.918	24900
UUG	L	0.181	18.571	27333	UAU	Y	0.439	13.223	19461
AUG	M	1	26.992	39727	UAA	*	0.65	2.023	2977
AAC	N	0.561	23.211	34161	UAG	*	0.196	0.608	895
AAU	N	0.439	18.154	26719	UGA	*	0.154	0.48	706

Supplementary Table 3. *V. natriegens* codon usage. Codon usage derived from genome sequence of *V. natriegens* ATCC 14048; RefSeq NZ_CP009977-8

Plasmid	Key Components	Origin of Replication	Selective Marker	Source
pRSF-PLtetO-GFP	GFP	RSF1010	Ampicillin	This study
pRSF-ParaB-spCas9-gRNA	Cas9, gRNA	RSF1010	Ampicillin	This study
pRSF-ParaB-dCas9-gRNA	dCas9, gRNA	RSF1010	Ampicillin	This study
pdCas9-bacteria	dCas9	p15A	Chloramphenicol	Addgene #44249
pCTX-R6K-gRNA	gRNA	CTX	Spectinomycin	This study
pCTX-RF	CTX replicative form	CTX	*Kanamycin*	[3]
pRSF-PlacUV5-tfoX	Induction of natural competence	RSF1010	Ampicillin	This study

Supplementary Table 4. Plasmids used in this study.

References

1. Hamashima, H., Iwasaki, M. & Arai, T. A Simple and Rapid Method for Transformation of Vibrio Species by Electroporation. in *Electroporation Protocols for Microorganisms* (ed. Nickoloff, J. A.) 155–160 (Humana Press).
2. Katashkina, J. I. *et al.* Use of the λ Red-recombineering method for genetic engineering of Pantoea ananatis. *BMC Mol. Biol.* **10**, 34 (2009).
3. Waldor, M. K. & Mekalanos, J. J. Lysogenic conversion by a filamentous phage encoding cholera toxin. *Science* **272**, 1910–1914 (1996).
4. Davis, B. Filamentous phages linked to virulence of Vibrio cholerae. *Curr. Opin. Microbiol.* **6**, 35–42 (2003).
5. Bernstein, D. A., Zittel, M. C. & Keck, J. L. High-resolution structure of the E.coli RecQ helicase catalytic core. *EMBO J.* **22**, 4910–4921 (2003).
6. Peters, J. M. *et al.* A Comprehensive, CRISPR-based Functional Analysis of Essential Genes in Bacteria. *Cell* **165**, 1493–1506 (2016).
7. Saha, A., Haralalka, S. & Bhadra, R. K. A naturally occurring point mutation in the 13-mer R repeat affects the oriC function of the large chromosome of Vibrio cholerae O1 classical biotype. *Arch. Microbiol.* **182**, 421–427 (2004).
8. Heidelberg, J. F. *et al.* DNA sequence of both chromosomes of the cholera pathogen Vibrio cholerae. *Nature* **406**, 477–483 (2000).
9. Egan, E. S. & Waldor, M. K. Distinct replication requirements for the two Vibrio cholerae chromosomes. *Cell* **114**, 521–530 (2003).
10. Qi, L. S. *et al.* Repurposing CRISPR as an RNA-guided platform for sequence-specific

control of gene expression. *Cell* **152**, 1173–1183 (2013).